Available online at www.sciencedirect.com
SCIENCE DIRECT
Polymer 47 (2006) 6099–6106
polymer
www.elsevier.com/locate/polymer

Shear-induced fractal morphology of immiscible reactive polymer blends

S. Patlazhan [a], G. Schlatter [b,*], C. Serra [b], M. Bouquey [b], R. Muller [b]

[a] *Semenov Institute of Chemical Physics of Russian Academy of Sciences, 4, Kosygin Street, Moscow 119991, Russia*
[b] *Laboratoire d'Ingénierie des Polymères pour les Hautes Technologies, UMR 7165, Departement Polymeres, Université Louis Pasteur, ECPM, 25, Rue Becquerel, 67087 Strasbourg Cedex 2, France*

Received 4 April 2006; received in revised form 19 June 2006; accepted 28 June 2006
Available online 17 July 2006

Abstract

The origin of shear-induced morphology of two-component immiscible reactive polymer blends is studied by the example of grafting and crosslinking multilayer systems of statistic terpolymer of ethylene, butyl acrylate, and maleic anhydride and statistic copolymers including polyamide and acid groups terminated by acid and/or amine groups. It is found that in contrast to the non-reactive system, the reactive polymer blends display pronounced hydrodynamic instabilities followed by the formation of branched fingers. The observed morphologies are shown to evolve towards the fractal structures. Their fractal dimensions depend on the type of chemical interactions between the blend components resulting either in grafted or crosslinked interfaces. It is shown that the obtained morphologies resemble the Laplacian growth patterns. A simple model of the interface chemical modifications is discussed to explain a physical origin of the observed shear-induced finger instability.

Keywords: Reactive immiscible polymer blends; Morphology; Fractal structure

1. Introduction

The interest in immiscible polymer blends has been growing since 1970s due to the relative easiness of their utilization in the manufacture of composite materials with the desired characteristics [1]. Physical and mechanical properties of such materials are shown to correlate considerably with their current morphology. Numerous studies were carried out to understand the mechanisms of structural development during processing (see, for example, [2–5]). They mostly deal with stability analysis and formation of different structural elements as lamellas, fibers, droplet, etc. Polymer blend morphologies depend to a great extent on the characteristics of interface between conjugated phases. Specifically, chemical modification of polymer chains by reactive groups may lead to grafting or crosslinking of interfaces of immiscible polymers. Owing to a local compatibility and reduction of interfacial tension, the reactive polymer blends show fine microstructure. Besides, grafting or crosslinking enhances adhesion between blend components and improves mechanical and some physical properties of the resulted composite materials [6–10]. The interface between reactive components is also sensitive to thermal fluctuations providing essential roughening [11,12].

This paper considers morphology formation of immiscible reactive polymer blends subjected to shear flow. The interest to this subject was motivated by recent observations revealing a great difference in morphologies of non-reactive, grafted, and crosslinked interfaces inherent to blends of statistical terpolymer of ethylene, butyl acrylate, and maleic anhydride with three types of copolymers including polyamide and acid groups terminated by acid and/or amine groups. Specifically, in contrast to the non-reactive system, the reactive polymer blends display distinct hydrodynamic instabilities induced by shear flow (cf. Fig. 4a–c). Furthermore, a closer examination of the observed structures reveals their similarity with the so-called viscous fingers, usually observed in the Hele-Shaw cell by the injection of less viscous fluid into a fluid of higher viscosity [13,14]. This type of instability arises when rates of

* Corresponding author. Tel.: +33 390 242 703; fax: +33 390 242 716.
E-mail address: Guy.Schlatter@ecpm.u-strasbg.fr (G. Schlatter).

0032-3861/$ - see front matter © 2006 Elsevier Ltd. All rights reserved.
doi:10.1016/j.polymer.2006.06.062

interfacial points are defined by local pressure gradient, ∇p. For the incompressible Newtonian fluids the Laplace equation $\nabla^2 p = 0$ holds true. For this reason the observed structures are called Laplace growth patterns [13,19–23]. These patterns were examined by the examples of different systems including reactive fluids [24–27]. Particularly, it was indicated that modification of surface tension by chemical reactions results in variation of fractal dimension of viscous fingers [25]. In this work we show that shear-induced structures of studied reactive polymer blends are regarded to the Laplacian growth patterns. A simple physical model is proposed to explain the origin of these instabilities.

2. Experimental section

2.1. Materials

The following reactive polymers were used: (i) statistic terpolymer of ethylene, butyl acrylate, and maleic anhydride labeled as MAH and (ii) three statistic copolymers including polyamide and acid groups PA6, PA6.9, PA11, and PA12 (the sample codes are CPA_C, CPA_G and CPA_{NR}). The MAH includes an average of 2.6 maleic anhydride groups randomly distributed along a chain. The CPA copolymers have been obtained using the same diacid and diamine monomers by polycondensation. The end-groups were controlled by varying the stoichiometric ratio of these monomers. Compositions of CPA polymers have been obtained by acid–base titration and are summarised in Table 1. CPA polymers are predominantly terminated by (i) two acid functions (CPA_{NR}), (ii) one acid − at the one end and one amine function − at the other (CPA_G), as well as (iii) two amine functions (CPA_C). The peculiarities of chemical reactions between MAH's maleic anhydride groups and CPA's amine functions allow us to separate polymer blends studied in (i) the non-reactive MAH–CPA_{NR} blend (marked as M_0-system), (ii) the grafted MAH–CPA_G blend (M_1-system) and (iii) the crosslinked MAH–CPA_C blend (M_2-system).

All experiments (rheological measurements and sample preparation) were carried out at 105 °C, which is well above the temperature needed for a chemical reaction between maleic anhydride and amine groups.

The complex viscosities of MAH and CPA_C polymer melts are presented in Fig. 1 as functions of the applied frequency. They were measured by ARES rheometer (TA-Instrument) equipped with oscillatory parallel plates. It was found that the diacid copolymer CPA_{NR} shows the same viscosity behavior as the diamine copolymer CPA_C. However, rheological characterization of CPA_G copolymer was difficult to carry out because of definite increase in its viscosity observed during measurements. This behavior is caused by chemical reactions between copolymer amine and acid terminal groups resulting in some increase of CPA_G molar weight.

Table 1
Polymer composition used for the study

	M_w (kg/mol)	Molar fraction of maleic anhydride function (mol/kg)	Molar fraction of terminal amine function (mol/kg)	Molar fraction of terminal acid function (mol/kg)
MAH	89	0.01	–	–
CPA_{NR}	60	–	0.047	0.349
CPA_G	60	–	0.088	0.119
CPA_C	60	–	0.254	0.044

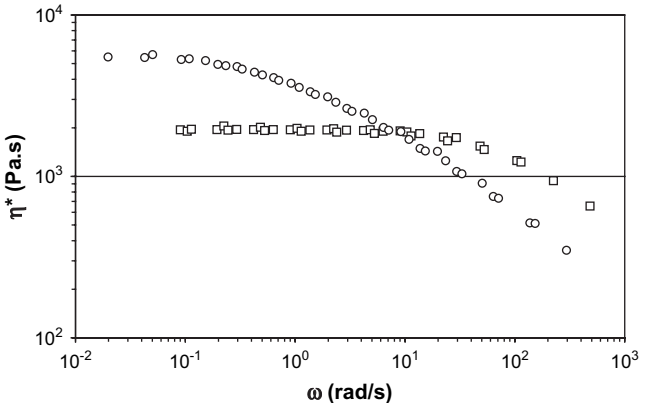

Fig. 1. MAH (○) and CPA_C (□) complex viscosities versus frequency at 105 °C.

2.2. Sample preparation

Each reactive copolymer was subjected separately to a compression molding to a disc-like form. The discs were cut across diameter and the half-discs of polyamide-bearing copolymers were then brought to contact with the half-disc of MAH terpolymer as shown in Fig. 2a. These compositions were placed between parallel plates of rheometer of radius $R = 12.5$ mm. To get a tight contact with the plates, sample thickness was reduced up to $h = 1.9$ mm. Then the upper plate was brought to a steady rotation producing multilayer morphology of the given polymer composition. The mean thickness d of the layers was controlled by the applied shear strain (Fig. 2b and c). Its value is a function of processing time t and distance R from the revolution axis,

$$d = \frac{\pi R}{\dot{\gamma}(R)t}, \tag{1}$$

where $\dot{\gamma}(R)$ is the corresponding shear rate which is dependent on the plate angular velocity Ω as $\dot{\gamma}(R) = R\Omega/(2\pi h)$. As long

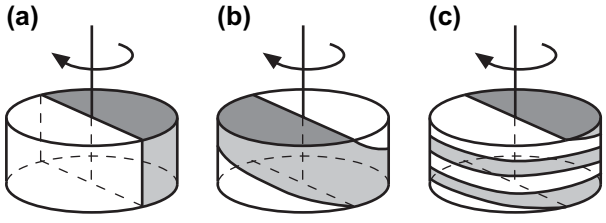

Fig. 2. Preparation of multilayer systems of two immiscible polymers clamped between parallel plates: initial configuration (a), half turn (b), and two turns (c).

as the shear rate is proportional to R, the mean layer thickness is independent of the distance from the revolution axis. The samples were prepared under the angular velocity $\Omega \cong 0.95$ rad/s during 600 s thus leading to $d \cong 65$ μm.

The following types of interfaces were obtained in the course of sample preparation:

- Non-reactive interface (M_0-system) of MAH–CPA_{NR} blend.
- Grafted interface (M_1-system) formed by anchoring CPA_G chains to reactive functional groups of MAH terpolymer (see Fig. 3a).
- Crosslinked interface (M_2-system) formed due to chemical bonding of CPA_C copolymer functional ends to MAH reactive groups (Fig. 3b).

2.3. Electron microscopy

To examine the obtained morphologies, the samples were sliced up to thin films under the liquid nitrogen temperature and studied by means of environmental scanning electron microscope (ESEM) Philips XL30/FEG. After collisions with atomic nucleuses a part of incident electrons bounces back into the vacuum. This back scattering was used to distinguish different types of copolymers thus revealing their interfaces.

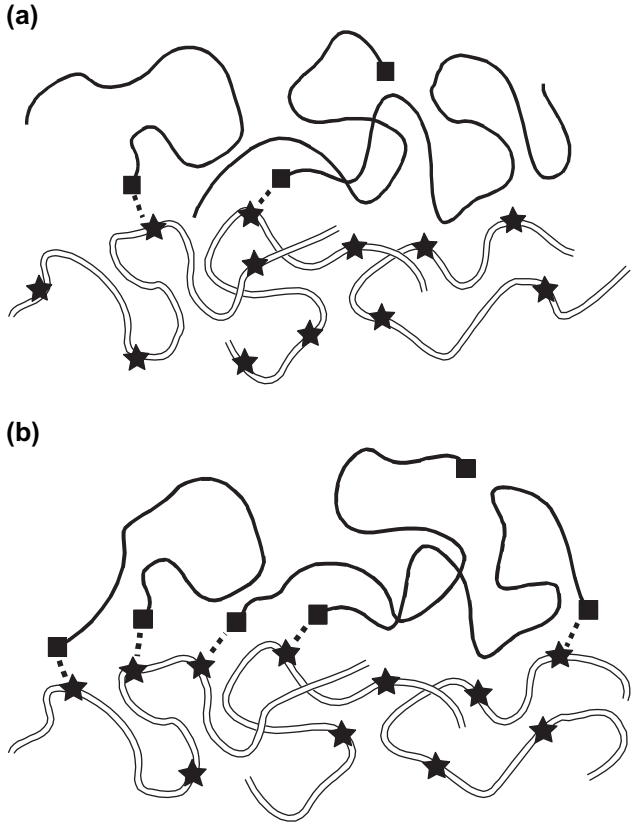

Fig. 3. Chemical structure of interface between reactive polymers: grafting MAH–CPA_G interface (a) and crosslinking MAH–CPA_C interface (b). The dotted lines denote chemical links.

3. Results and discussion

3.1. Fractal interface morphology

The typical morphologies of the considered multilayer systems are presented in Fig. 4. They correspond to peripheral cuts of the samples where shear stresses reach maximum. The black areas represent maleic anhydride (MAH) while white regions are filled by CPA copolymers. One can see that shearing of the non-reactive M_0-system leads to a multilayer structure with relatively smooth interface (Fig. 4a). On the contrary, both reactive polymer blends, M_1- and M_2-systems, demonstrate totally different morphologies characterized by crumpled interfaces (Fig. 4b and c). A careful examination of these interfaces reveals specific branched formations of many-scale hierarchy. The M_2-system with the crosslinked interface shows more pronounced large-scale disturbances. Their details are enlarged in Fig. 4d. The shape of these disturbances reminds somehow of classical viscous fingering in the Hele-Shaw cell under injection of a less viscous fluid into a more viscous one [13,14]. As long as viscous fingers represent the fractal objects, we can assume that the observed shear-induced morphologies of reactive polymer blends studied also belong to fractal patterns. In order to confirm this assumption the box-counting method [14,15] was used to measure fractal dimensions. In this method, a grid of squire boxes of r in size is used to cover the tested area. The number N_r of boxes intersecting the studied structures is regarded as a function of different box sizes. The resulting N_r is then plotted versus r in a double logarithmic coordinates. If an analyzed pattern represents a fractal object, the linear $\log(N_r)$–$\log(r)$ dependence is valid. Its slope corresponds to a fractal dimension, D_f, of a structure.

To apply this method to electron-microscope images of Fig. 4, the grey domains were converted to black-and-white patterns. Fig. 5 shows that linear $\log(N_r)$–$\log(r)$ dependences occur within the size range between 2 μm and 60 μm for both of the reactive polymer blends. This result confirms our conjecture that structures of sheared M_1- and M_2-systems fall into the category of fractal patterns. The analysis reveals that grafted interface (M_1-system) is characterized by the fractal dimension $D_f = 1.75$ while crosslinked interface (M_2-system) is described by $D_f = 1.84$. These characteristics are rather close to $D_f = 1.7$ which is peculiar to fractal dimension of 2D Laplacian growth patterns exemplified by viscous fingering, invasion percolation, diffusion-limited aggregates and dielectric breakdown [13–18].

3.2. Mechanism of interface instability in reactive polymer blends

To get more insight into the physical origin of the observed shear-induced patterns, the normal force N has been recorded during the development of multilayer structures. It was found that the normal force does not change with shearing of the non-reactive M_0-system. It means that growth of number of layers does not influence mechanical response of this system. On the other hand, the normal force evolves significantly for

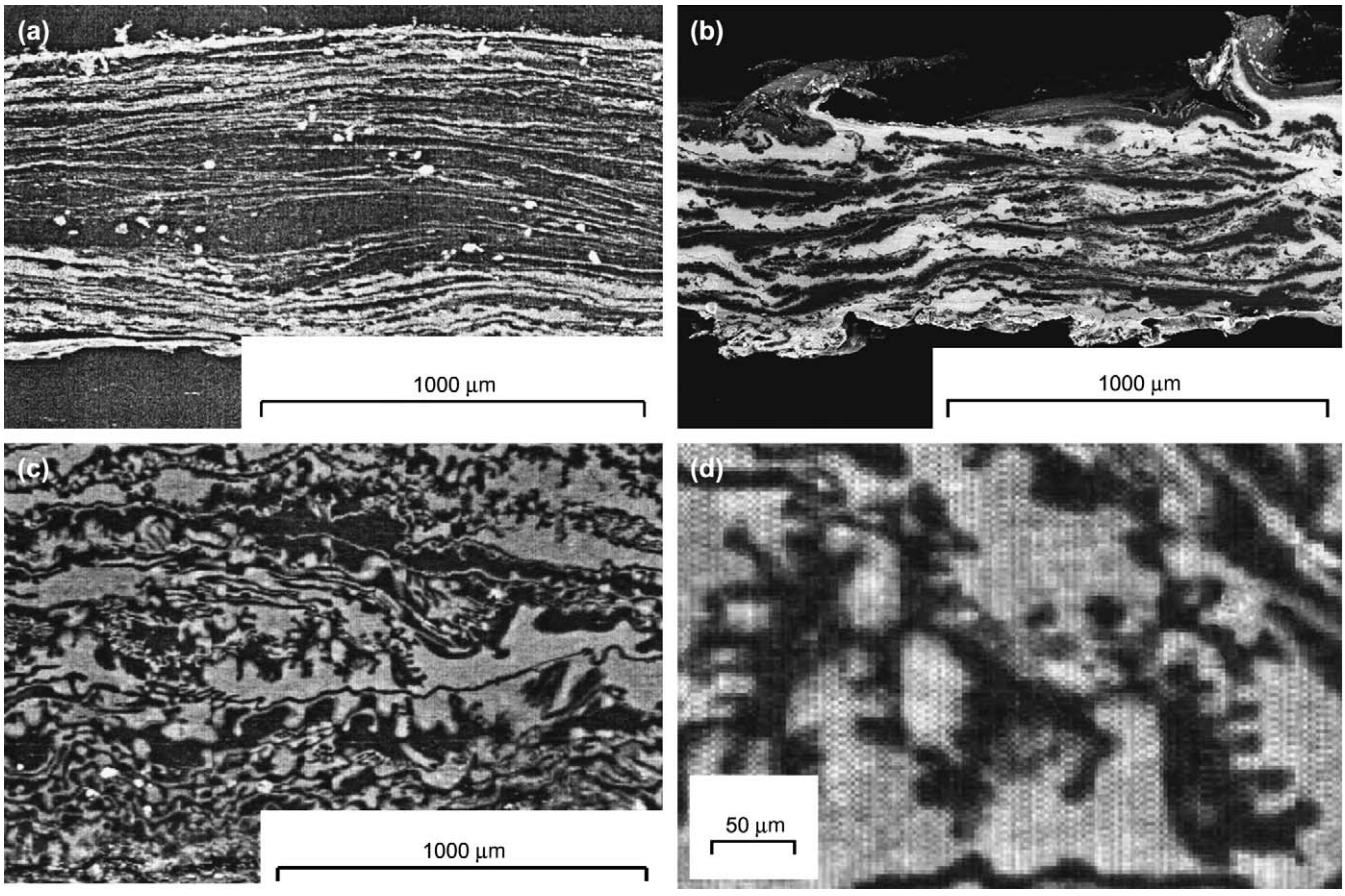

Fig. 4. Scanning electron microscopy images of three types of multilayer systems: MAH–CPA_{NR} blend with non-reactive interface (a), MAH–CPA_G blend with grafted interface (b), and MAH–CPA_C blend with crosslinked interface (c) along with its enlarged image (d).

both reactive M_1- and M_2-systems considered: Fig. 6 reveals that after the plateau zones a continuous increase of the normal force occurs (the initial time of the plot corresponds to the sample configuration presented in Fig. 2a).

These changes are related to the hydrodynamic instabilities caused by the modification of interfacial properties (interfacial tension and elasticity) due to the chemical reactions between the CPA's amine and MAH's maleic anhydride groups. In order to understand these data we should clarify the origin of the observed shear-induced finger-like formations. As mentioned, they resemble to viscous fingers arising in the Hele-Shaw cell under the local pressure drop between two fluids. This analogy brings up the question: how may pressure drops occur in the stratified system under the simple shear flow? It is reasonable to imagine that in the absence of hydrodynamic instability caused by the distinction in viscoelastic properties of polymer layers (cf. morphology of the non-reactive

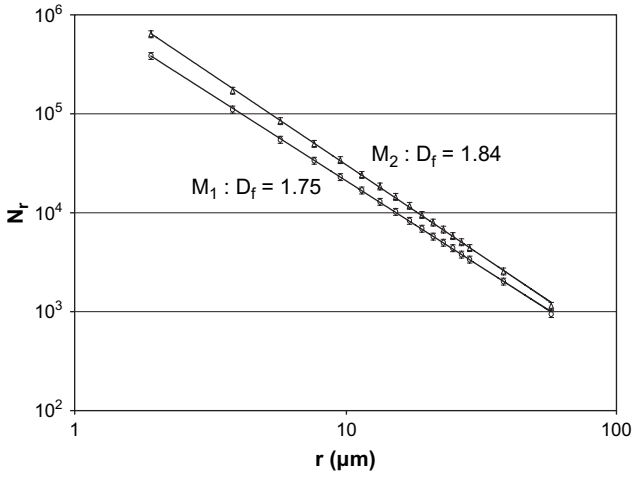

Fig. 5. The $\log(N_r)$ to $\log(r)$ dependences for grafted (M_1-system) and crosslinked (M_2-system) polymer blends obtained by box-counting method. The fractal dimensions D_f are obtained by linear approximation of measured points in the range from 2 μm to 60 μm.

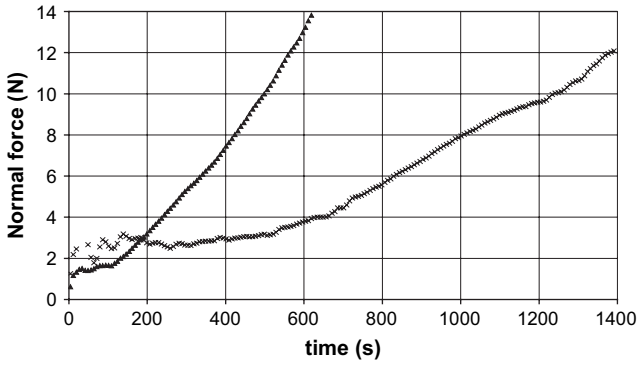

Fig. 6. Time evolution of the normal force N under shearing of the multilayer: MAH–CPA_C (▲) and MAH–CPA_G (×) systems at 105 °C and $\dot{\gamma} = 1\ s^{-1}$.

M_0-system shown in Fig. 4a), the only reason for local pressure drops is the heterogeneous interface structure appearing with chemical modification during shear flow.

To prove this assumption, first consider the reactive M_2-system with crosslinked interface. We suppose that interfacial crosslinking of polymer chains would affect neither hydrodynamic stability nor the normal force (plateau zone in Fig. 6) until the moment when rigidity of some reacted interfacial domains (sol clusters) reaches the definite value allowing to keep their shape under the influence of small perturbations. These clusters will be called as solid-like domains. Due to density fluctuations of the crosslinked chains, the other parts of interface will be covered by dispersed soft clusters or unreacted chains. These parts will be named as liquid-like windows.

At rest, the interfacial crosslink density will be quickly homogenized due to the different mobilities of the crosslinked and the free chains. However, if shear flow is applied, local pressure drops will be induced in the liquid-like windows (see Section 3.3). This will result in pushing of one polymer fluid to another one leading to sharp interface perturbations (see Figs. 8 and 9). On the other hand, these splashes increase interfacial area thus diminishing the crosslink density within the liquid-like windows. This will strengthen interface heterogeneity, which is favourable for increasing pressure drops and gives rise to the viscous fingering. Hence, the discussed phenomenon is governed by the competition between hydrodynamic instabilities and kinetics of interfacial chemical reactions. A comprehensive modeling of these processes is rather complicated and yet to be studied. For this reason in Section 3.3 we are restricted by a model approach and study shear-induced instability within the single liquid-like window.

In the case of grafting (M_1-system), the solid-like domains may appear only at sufficiently large concentration of the nascent polymer brush when the mean distance between graft points becomes smaller than the gyration radii of polymer chains. In this instance the interface copolymers are being stretched thus providing the bending resistance. It is clear that the creation of such brush domains needs much more time as compared with crosslinked clusters. This clarifies why the plateau zone of the grafted M_1-system is longer than that of the crosslinked M_2-system.

The long waiting period should also decrease the dimension of liquid-like domains having sparse hair. This is confirmed by the image of the grafted MAH–CPA_G blend showing shorter fingers than the crosslinked MAH–CPA_C blend (cf. Fig. 4b and c). The existence of a fraction of diamine-terminated chains may result in the presence of some crosslinked polymer in the M_1-system. It should not influence the mechanism of instability proposed. The increase of the crosslinked polymer fraction in the grafted blend may just decrease the plateau zone.

3.3. Numerical modeling of interface instability due to shear-induced pressure drop

To estimate the effect of the shear-induced pressure drop in the interface liquid-like domain, one considers a 2D model of two-layer fluids of equal thicknesses h and densities ρ but of different viscosities, η_l and η_u, of the lower and the upper layers, respectively (see Fig. 7b). The molten polymers are considered incompressible and obey Newtonian behavior under the applied shear rate of 1 s^{-1}. Fig. 1 shows that for CPA copolymer while MAH terpolymer is in the non-Newtonian regime at that shear rate. However, for qualitative predictions, the assumption of Newtonian behavior is sufficient because the imbalance of elasticity between the two phases cannot in itself be the origin of hydrodynamic instability because unreactive system does not show it.

The layers are separated by the heterogeneous interface containing the liquid-like window of width L between the two solid-like domains. The flow time is supposed to be much smaller than the characteristic time of the domain formation. In this condition L may be kept fixed. The hydrodynamic behavior of this system is governed by the Navier–Stokes and mass conservation equations:

$$\rho\frac{\partial \mathbf{u}}{\partial t}+\rho(\mathbf{u}\cdot\nabla)\mathbf{u}=-\nabla p+\eta\Delta\mathbf{u}-\sigma\kappa\mathbf{n}\delta, \tag{2}$$

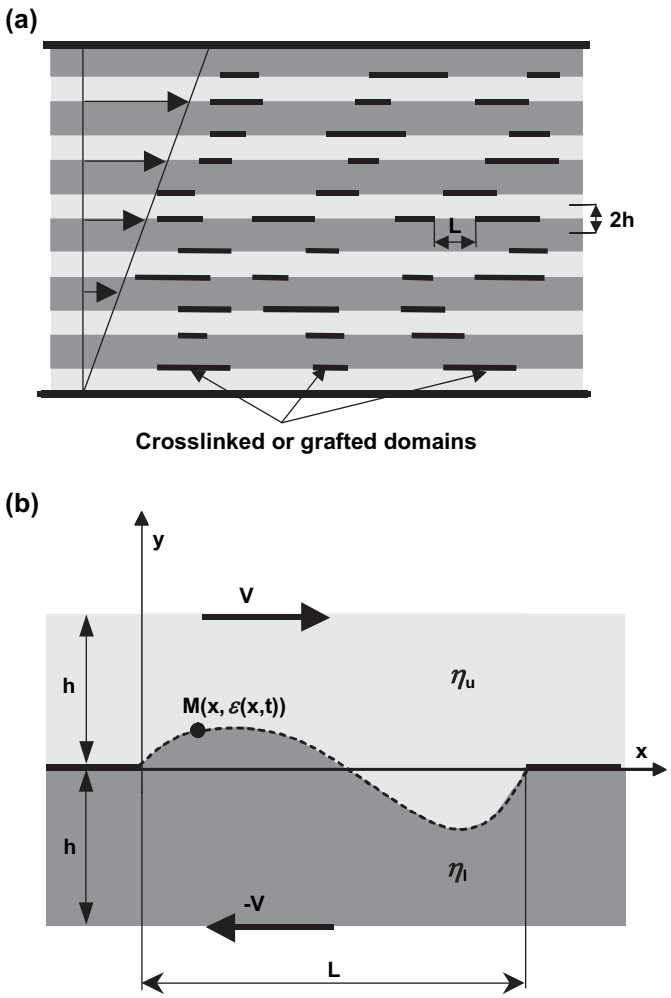

Fig. 7. Schematic representation of a reacted multilayer system (a) and liquid-like window located between solid-like (crosslinked or grafted) domains of interface (b).

$$\nabla \cdot \mathbf{u} = 0 \tag{3}$$

Under the following boundary conditions for the velocity field $\mathbf{u}$:

$$\mathbf{u}(x, y = h) = -\mathbf{u}(x, y = -h) = \mathbf{V}, \tag{4}$$

$$\mathbf{u}(x = 0,\ y) = \mathbf{u}(x = L,\ y) = \mathbf{V}\frac{y}{h}. \tag{5}$$

$\mathbf{V}$ and $-\mathbf{V}$ are the velocities of the upper and lower boundaries of the layers. The last term of Eq. (2) corresponds to the surface force density due to the interfacial tension σ; κ and $\mathbf{n}$ are the local curvature and unite normal to the interface directed outwards of the lower fluid, respectively (cf. Fig. 7b); δ is the interfacial delta function. Gravity forces are considered negligible as compared with viscous forces. The coordinate frame is considered to move with solid-like domains. Eq. (5) reflects the condition of the undisturbed shear rate at the lateral boundaries of the liquid-like window.

A level set method was applied to compute the interface evolution [28]. This implies tracking of the moving interface by means of a continuous level set function $c(x,y,t)$ defined at any time t in each point $M(x,y)$ of the considered domain as (see also Fig. 7):

$$c(x,y,t) = \begin{cases} c(x,y,t) > 1/2 \text{ for } M \in \text{lower fluid} \\ c(x,y,t) < 1/2 \text{ for } M \in \text{upper fluid} \\ c(x,y,t) = 1/2 \text{ for } M \in \text{Interface} \end{cases}$$

In order to take into account the steep change in the viscosity η through the interface, a Heaviside function $H(c)$ is used:

$$\eta = \eta_l H(c) + \eta_u [1 - H(c)], \tag{6}$$

where $H(c)$ is defined as:

$$H(c) = \begin{cases} 0 & \text{at } c < 1/2 \\ 1/2 & \text{at } c = 1/2 \\ 1 & \text{at } c > 1/2 \end{cases} \tag{7}$$

The evolution of the level set function $c(x,y,t)$ along with the development of interfacial instability is governed by the following advection equation:

$$\frac{\partial c}{\partial t} + (\mathbf{u} \cdot \nabla)c = 0. \tag{8}$$

The inflow boundary conditions related to the level set function are as follows:

$$c(x = 0,\ y > 0) = 0 \text{ and } c(x = L,\ y < 0) = 1 \tag{9}$$

While the outflow boundary conditions are defined by the convective fluxes as:

$$\mathbf{n} \cdot \nabla c|_{x=0,\ y<0} = \mathbf{n} \cdot \nabla c|_{x=L,\ y>0} = 0 \tag{10}$$

where $\mathbf{n}$ is the unit normal to the interface. Interface is assumed to be unperturbed at the initial moment $t = 0$:

$$c(t = 0,\ 0 < x < L,\ y > 0) = 0 \text{ and } c(t = 0,\ 0 < x < L,\ y < 0) = 1 \tag{11}$$

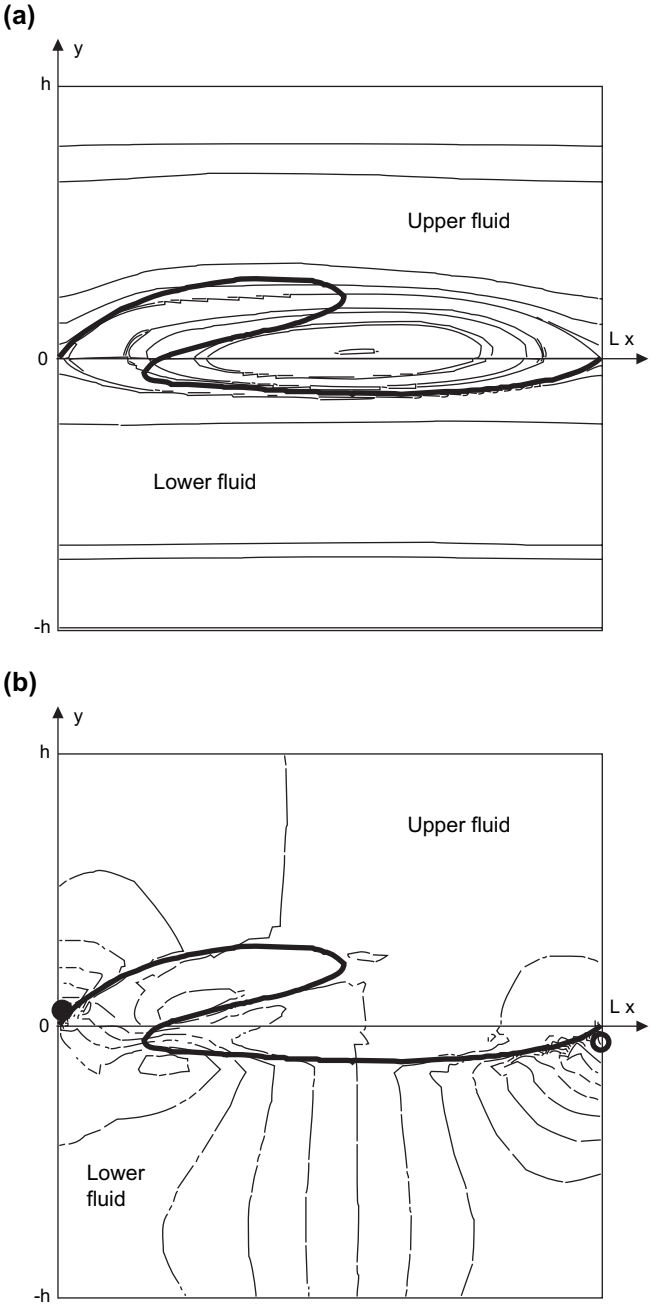

Fig. 8. Stream lines and pressure distribution in a vicinity of liquid-like window after 8 s of shear flow: (a) the velocity streamlines and (b) iso-pressure levels are drawn with thin lines. The thick line represents the interface position. Symbols (●) and (○) correspond to pressure maximum and minimum locations, respectively. The viscosity ratio is $\eta_l/\eta_u = 8$. The window sizes are $2h = L = 100$ μm.

The boundary value problem (Eqs. (2)–(11)) has been solved with the finite elements method using Femlab™ software. In order to reduce unrealistic numerical oscillations of the level set function near the interface, Eq. (8) was treated by means of streamline upwind Petrov–Galerkin (SUPG) method.

The velocity streamlines calculated for liquid-like window of sizes $L = 2h = 100$ μm are presented in Fig. 8a (thin lines) for the following material and flow parameters: viscosity ratio

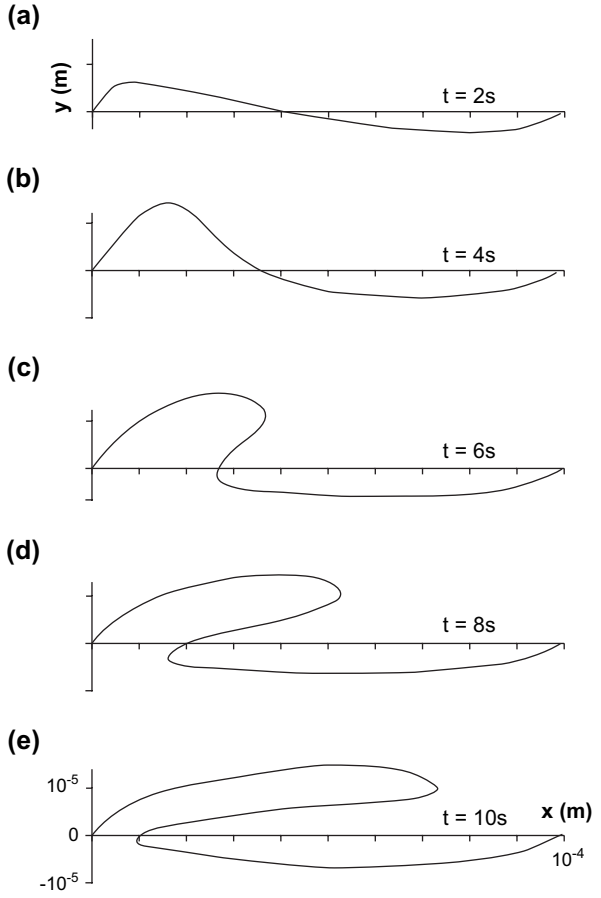

Fig. 9. Time evolution of liquid-like interface: $t = 2$ s (a), $t = 4$ s (b), $t = 6$ s (c), $t = 8$ s (d), and $t = 10$ s (e). The system parameters are the same as in Fig. 8.

$m = \eta_l/\eta_u = 8$, interfacial tension $\sigma = 0.05\ \mathrm{N\,m^{-1}}$, and shear rate $\dot{\gamma} = 1\ \mathrm{s^{-1}}$. It has been shown that the interfacial tension has no significant effect because for the given parameters capillary number is far more than unity. This results in viscous forces well over capillary forces. The streamlines correspond to circulatory velocity field leading to interface disturbances (thick line in Fig. 8a). The iso-pressure levels are presented in Fig. 8b (thin lines) along with the interface profile (thick line) at the same processing time as Fig. 8a. This illustrates that a local pressure gradient is developing in a vicinity of the interface despite the fact that global flow is a simple shear. This effect gives rise to the observed instability (see Fig. 9 showing evolution of interface disturbances with processing time). It is seen that more viscous fluid is extended to a less viscous upper layer more sharply than in the reverse case. This is explained by the fact that pressure developed in a more viscous layer is higher than that in a less viscous layer. It is worthwhile to note that the opposite effect takes place in viscous fingering in the Helle-Shaw cell: the branching structure is developed while a less viscous liquid is injected to a more viscous one.

The effect of viscosity ratio is shown in Fig. 10. It results in growth of interface perturbations with the increase of viscosity ratio m. Particularly, it is seen that the interface disturbance is

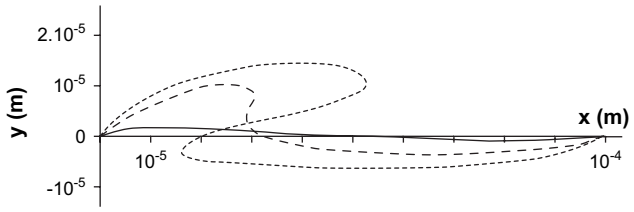

Fig. 10. Effect of the viscosity ratio η_l/η_u on the interface position after 8 s of shear flow: $\eta_l/\eta_u = 1.5$ (solid line); $\eta_l/\eta_u = 3$ (dashed line); $\eta_l/\eta_u = 8$ (dotted line).

essential for $m = 3$ corresponding to our experimental case. Its shape reminds somehow of the details of shear-induced structure of the crosslinked M_2-system shown scaled-up in Fig. 4d. The resulted viscous finger grows and deforms in shear flow (cf. Fig. 9). On the other hand, it will result in extension of interface specific area. This process in its turn will favor in formation of new finite crosslinked domains alternated by liquid windows of smaller sizes producing fingers of the second generation, etc. As a result, a fractal branched structure will appear.

4. Conclusion

Regularities of development of shear-induced morphology of non-reactive and reactive two-component multilayer systems are studied by processing of statistic terpolymer of ethylene, butyl acrylate, and maleic anhydride and statistic copolymers including polyamide and acid groups terminated by acid and/or amine groups. Depending on the ratio of the amine and the maleic anhydride groups the samples comprise unreacted, grafted, or crosslinked interfaces. The reactive polymer systems display considerable hydrodynamic instabilities followed by the branched finger-like formations while the non-reactive system follows the unperturbed flow. The developed morphologies of the reactive polymer blends correspond to fractal structures within the range between 2 μm and 60 μm. The fractal dimensions of the crosslinked and grafted systems are equal to $D_f = 1.84$ and $D_f = 1.75$, respectively. These values are close to the fractal dimension of the Laplacian growth patterns. The heterogeneous character of interface modification during crosslinking or grafting provides a physical origin of the observed instabilities: the formation of chemically modified (solid-like) and unmodified (liquid-like) domains results in considerable local pressure gradients promoting injection of one polymer fluid to another and leading to the shear-induced fingering.

Acknowledgments

The authors wish to thank Dr. Benoit Ernst and Dr. François Coupart from CERDATO laboratory of ARKEMA for having provided the samples and done the microscopy. S.P. expresses his gratitude for hospitality during his work at the Polymer Department of ECPM. This work was partially supported by

the Russian Foundation of Basic Research (grant no. 05-03-33018).

References

[1] Utracki LA. Polymer alloys and blends. New York: Oxford University Press; 1990.
[2] Han CD, Yu TC. Polym Eng Sci 1972;12:81–90.
[3] Favis BD, Therrien D. Polymer 1991;32:1474–81.
[4] Bourry D, Favis BD. Polymer 1998;39:1851–6.
[5] Lee JK, Han CD. Polymer 1999;40:6277–96.
[6] Shonaike GO, Simon GP. Polymer blends and alloys. New York: Marcel Dekker; 1999.
[7] Baker WE, Scott CE, Hu GH. Reactive polymer blending. Hanser Gardner; 2001.
[8] Guégan P, Macosko CW, Ishizone T, Hirao A, Nakahama S. Macromolecules 1994;27:4993–7.
[9] Kim S, Kim JK, Park CE. Polymer 1997;38:1809–15.
[10] Legros A, Carreau PJ, Favis BD, Michel A. Polymer 1994;35:758–64.
[11] Yu X, Wu Y, Li B, Han Y. Polymer 2005;46:3337–42.
[12] Lyu SP, Cernohous JJ, Bates FS, Macosko CW. Macromolecules 1999;32:106–10.
[13] Random fluctuations and pattern growth: experiments and models. In: Stanly HE, Ostrowsky N, editors. Proceedings of NATO advanced study institute, series E, vol. 157. Dordrecht, Boston, London: Kluwer Academic Publishers; 1988.
[14] Vicsek T. Fractal growth phenomena. Singapore: World Scientific; 1992.
[15] Block A, von Bloh W, Schellnhuber HJ. Phys Rev A 1990;42:1869–74.
[16] Paterson L. Phys Rev Lett 1984;52:1621–4.
[17] Måløy KJ, Feder J, Jøssang T. Phys Rev Lett 1985;55:2688–91.
[18] Homsy GM. Annu Rev Fluid Mech 1987;19:271–311.
[19] Shraiman B, Bensimon D. Phys Rev A 1984;30:2840–2.
[20] Lenormand R, Zarcone C. Phys Rev Lett 1985;54:2226–9.
[21] Howison SD. J Fluid Mech 1986;167:439–53.
[22] Vespignani A, Pietronero L. Phys A 1991;173:1–21.
[23] Hentschel HGE, Levermann A, Procaccia I. Phys Rev E 2002;66:016308.
[24] Pojman JA, Gunn G, Patterson C, Owens J, Simmons C. J Phys Chem B 1998;102:3927–9.
[25] Fernandez J, Homsy GM. J Fluid Mech 2003;480:267–81.
[26] Nagatsu Y, Ueda T. Chem Eng Sci 2004;59:3817–26.
[27] De Wit A, Homsy GM. J Chem Phys 1999;110:8663–75.
[28] Sussman M, Osher S. J Comput Phys 1994;114:146–59.